JMEPEG (2021) 30:7636–7644
https://doi.org/10.1007/s11665-021-05900-3

1059-9495/$19.00

Effect of Tool Rotational Speed on the Microstructure and Associated Mechanical Properties of Incrementally Formed Commercially Pure Titanium

G. Yoganjaneyulu, S. Vigneshwaran, R. Palanivel, Adel Alblawi, Mohammad Abdur Rasheed, and R.F. Laubscher

Submitted: 17 February 2021 / Revised: 18 April 2021 / Accepted: 1 May 2021 / Published online: 24 May 2021

Single-point incremental forming (SPIF) was conducted on a 1-mm-thick commercially pure titanium grade 2 (Ti-G2) sheet metal in a CNC vertical milling unit. A hardened steel ball of 12 mm diameter was used as forming tool. Frustum cups were formed with varying spindle speeds between 300, 450, and 600 RPM. Other process parameters including the vertical step down and feed rate were kept as 0.2 mm and 300 mm/min, respectively. The metallurgical and mechanical properties of the formed material were investigated by cutting samples from the frustum cup walls. Electron-backscattered diffraction (EBSD) investigation revealed limited change in grain size with an increase in spindle speed. Dislocation density was measured by x-ray diffraction peak broadening analysis. The results indicate that an increase in spindle speed resulted in an increased dislocation density. The EBSD-based textural studies revealed a strong basal texture with near P and B type orientations visible at the maximum spindle speed. The tensile tests demonstrated a proportional increase in tensile strength with an increase in spindle speed along with a significant reduction in total ductility. The enhanced dislocation density and the formation of a strong basal texture were considered as the main drivers for the improvement in the tensile strength. A maximum tensile strength of nearly 550 MPa was obtained for samples extracted from the walls of the frustum cup at the maximum spindle speed of 600 RPM. This translates to an 80% enhancement of the tensile strength when compared to the base metal .

Keywords electron-backscattered diffraction, mechanical properties, microstructure, single-point incremental forming, titanium, tensile testing

1. Introduction

The titanium grade 2 (Ti-G2) is considered as the workhorse of the chemical and piping industry where superior chemical resistance, excellent strength-to-weight ratio, good weldability, and good formability are required (Ref 1). Its uses include tubing or piping systems, gas and oil storage and delivery systems, pressure vessels, chemical reaction vessels, heat exchangers, liners and various other industrial applications (Ref 2). These applications may involve various forming operations. Ti and its alloys are successfully employed in these applications with achievable tolerance levels comparable to stainless steels. However, the tolerance achieved is inferior to that of steels. Ti-G2 (commercially pure grade) is mostly used for cold forming operations (Ref 3). The commercial pure grade of Ti exhibits typically hexagonal closed pack (HCP) crystal structures at low temperature and a body-centered cubic (BCC) crystal structure at elevated temperatures (above 800°C). Typically, the deformation of Ti occurs due to a twining-based mechanism and exhibits a different stress–strain behavior in tension and compression (strength differential effect) (Ref 4). Ti alloys are sensitive to strain rate and better formability is achieved when it is formed at low strain rates at ambient temperature. Efforts have been made by several researchers to understand the forming behavior of Ti and its alloys through the conventional punch stretch test (Ref 4-6) as well as through various incremental forming techniques (Ref 7-9). Unlike the conventional punch stretch test, the single-point incremental forming (SPIF) test utilizes a point contact on the sheet metal surface and incrementally conveys the desired shape on it. This necessitates specialized computer numerical control (CNC) forming equipment. SPIF does not require a conventional punch and die setup and only a relatively simple fixture support (Ref 10, 11). SPIF has been demonstrated to attain higher forming limits than any other conventional sheet metal forming processes. To capitalize on this potential elevated formability, it is essential to investigate how the process parameters affect the success of the forming process. The most significant process parameters in SPIF are sheet metal thickness, tool diameter, tool shape, vertical step down, spindle speed, and lubrication (Ref 12). The literature reports that formability may be increased with an increase in sheet metal thickness during SPIF (Ref 13, 14). Subsequent papers suggest an optimized sheet metal thickness resulting in improved formability (Ref 15). In line with the above, an increase in tool diameter (Ref 16-18) and an increase in spindle speed (Ref 16, 19) was also

G. Yoganjaneyulu, Advanced Metal Forming Laboratory, Department of Mechanical Engineering, Vignan's Institute of Information Technology, Visakhapatnam, Andhra Pradesh 530049, India; **S. Vigneshwaran**, Department of Mechanical Engineering, National Institute of Technology Puducherry, Karaikal 609609, India; **R. Palanivel** and **Adel Alblawi**, Department of Mechanical Engineering, College of Engineering, Shaqra University, P.O. 11911, Dawadmi, Ar Riyadh, Saudi Arabia; **Mohammad Abdur Rasheed**, Department of Civil Engineering, College of Engineering, Shaqra University, P.O. 11911, Dawadmi, Ar Riyadh, Saudi Arabia; **R.F. Laubscher**, Department of Mechanical Engineering Science, University of Johannesburg, Auckland Park Kingsway Campus, Johannesburg 2006, South Africa. Contact e-mail: svigneshwaranmech2010@gmail.com.

demonstrated to improve formability during SPIF of various sheet metals. Researchers also suggested that a decrease in both vertical step down and feed rate results in better formability (Ref 17-22). From the literature, it therefore inferred that an increase in tool diameter and spindle speed both have positive effects on formability whereas the increase in vertical step down and feed rate may affect the formability. The effect of SPIF process parameters on the formability of various metallic materials (Ref 12-14, 17, 19-21) and Ti alloys (Ref 16, 22, 23) has been investigated. However, there are no reports for Ti-G2 that correlate the SPIF process parameters with the mechanical properties obtained for the resulting incrementally formed components. In general, Ti-G2 displays higher formability as well as lower spring back when compared to the other commercial pure grades typically used. Also due to the lower mechanical properties of the commercially pure grades, when compared to the higher alloy grades, they are typically utilized in less structurally important applications (Ref 24). This paves the way to also improve their usability if the mechanical properties may be significantly enhanced by the incremental forming process.

Ajay (Ref 25) in a recent study reported that the significant process parameters for the SPIF process are the spindle speed, the vertical step down, and the feed rate. However, lowering the vertical step down and feed rate with moderate spindle speed resulted an optimal outcome in Ti alloys. The outcomes considered by the aforesaid author are the wall angle, surface roughness, and thinning. In our earlier report on SPIF of Ti-G2, the higher tool diameter and higher spindle speed produced better forming limit strain (Ref 16). From the other reports (Ref 17-22), it is understood that lower vertical step down and feed rate enhances formability in SPIF. Hence, for the present investigation, a higher tool diameter, lower vertical step down, and lower feed rate have been chosen to attain higher formability in the frustum cups and these parameters were unaltered during the entire study. Besides an attempt is made in this investigation, to primarily understand the effect of a spindle speed alone on the formability of Ti-G2. This is because the primary intention of this experimental study is to attain maximum formability in a shorter time interval, which can reduce the cycle time of the SPIF process. This is potentially possible by increasing the spindle speed. Furthermore, the subsequent mechanical properties of SPIF Ti-G2 frustum cups are experimentally evaluated in this study. The correlation between the properties and the structure resulting from the single-point incremental formed Ti-G2 frustum cups conducted at various spindle speeds can provide an insight about the mechanical properties attainable to eventually widen the potential applications for commercially pure Ti.

2. Experimental Procedure

2.1 Preliminary Testing of Base Metal (BM)

The chemistry (in wt.%) of the BM (Ref 9) is 0.03 N, 0.08 C, 0.014 H, 0.2 Fe, 0.17 O, and balance Ti. The tensile properties of the base metal were evaluated by tensile test. The samples for tensile test (microtensile) were prepared along the rolling direction of sheet metal using wire-cut electrical discharge machining (WEDM). The tensile tests were conducted with a crosshead speed of 1 mm/min using a Tinius Olsen 50KL tensile tester. Tensile properties were reported based on an average of three tensile tests conducted.

2.2 Single-Point Incremental Forming (SPIF)

In the present study, the sheet thickness of 1mm was chosen. Further, a constant tool diameter of 12 mm, vertical step down of 0.2 mm, and a feed rate of 300 mm/min was employed. The higher tool diameter produced higher forming limit strain, which was predicted experimentally from our earlier report (Ref 9). Hence, a tool diameter of 12 mm was chosen. After experimentally evaluating the various combinations of vertical step down (0.2, 0.4 and 0.6 mm) and feed rates (300, 600 and 900 mm/min), the lower value of vertical step down and feed rate was chosen, as it has produced higher formability in SPIF. However, it is not shown in the present study. The spindle speed was varied as 300, 450 and 600 rpm. Grease was used as a lubricant.

Forming specimen was manufactured by shearing the procured BM material (1-mm-thick sheet) into 150 mm squares. Circular grids of 2 mm diameter in a rectangular array were engraved to a depth of 0.05 ± 0.005 mm (on one side of the sheared sheet metal) using a laser-assisted unit. Laser-engraved sheet metals were secured in a specially fabricated fixture setup. A vertical milling CNC machine (GSK 928 MA) was employed to carryout SPIF (refer Fig. 1a). The tool comprised of a hardened steel ball (12 mm diameter) attached to the tool shank. The machine was coded to form the frustum cups at the various spindle speeds, i.e., 300, 450, and 600 rpm.

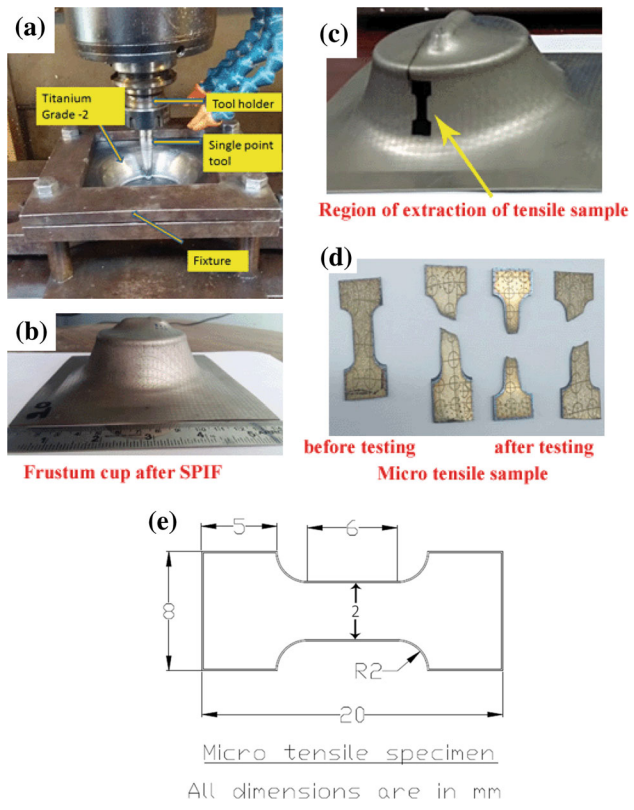

Fig. 1 (a) experimental setup for SPIF, (b) frustum cup obtained after SPIF, (c) region of extraction of tensile sample from the frustum cup, (d) microtensile samples (before and after tensile tests), and (e) Dimensional details of microtensile specimens (redrawn based on the work of Nadammal et al., 2015 (Ref 26)

However, the vertical step down was fixed as 0.2 mm while, the feed rate was kept as 300 mm/min. Grease (Molybdenum disulfide) were applied at the tool and blank contact area during SPIF. Frustum cups with a wall angle of 55° were formed based on the above parameters. SPIF continued until the Ti-G2 sheet metal displayed a fracture at the bottom edges of frustum cup (refer Fig. 1b).

2.3 Frustum Cup Strain Investigation

Completed frustum cups were investigated for limiting strains by referring to the circular engravings. The strains transformed the circular engravings into elliptical shapes from which it was possible to measure the major and minor axes of the ellipses to then infer the forming and fracture limiting strains. These results and analysis are reported elsewhere (Ref 9). Since the primary focus of this study is to investigate the mechanical properties of the formed material microtensile test, samples were prepared from the walls of the formed frustum cups (see Fig. 1c). Formed frustum cups typically have a near uniform wall thickness and therefore makes tensile testing possible. Tensile tests using a similar setup to the base metal testing (“Single-Point Incremental Forming (SPIF)” Section) were conducted on the frustum cup wall sourced specimen. The effect of spindle speed on the grain size distribution and misorientations, on a local scale, was examined by scanning electron microscopy with attached electron-backscattered diffraction (SEM-EBSD) detection. The samples for the EBSD investigation were also obtained from the walls of the frustum cup and were prepared manually to eventually be electropolished in a Struers-Electropol-IV at 38 V (DC) for 20s in the presence of 80% methanol and 20% perchloric acid electrolyte solution. The orientation image micrographs (OIM) were recorded by a FEI-Quanta 3D FEG-SEM with a step size of 0.3 μm. TSL OIM 4.6 software was used to analyze the EBSD maps. Additional 10 mm square specimen were also removed from the formed frustum cup walls to be used for the x-ray diffraction (XRD) studies. XRD was conducted on a Rigaku Ultima III unit with 1.5406 Å wavelength radiation source (Cu-Kα) and a fixed scan rate of 2°/min.

3. Results and Discussion

3.1 Microstructural Characterization

The microstructural characterization of the BM and the formed frustum cup specimen was conducted by SEM-based EBSD techniques. Inverse pole figure (IPF) maps, grain size distribution, and misorientation plots of the BM and subsequent SPIF specimen at the various spindle speeds are presented in Fig. 2(a-l). Figure 2(a) represents the standard stereographic representation, which indicates the orientation of grains shown in IPF maps. The color legend map is common for all the IPF maps presented in Fig. 2. The appearance of grains in the BM (refer Fig. 2a) shows near equiaxed grains and resembles a rolled microstructure, mostly, as the BM was procured as a sheet metal (Ref 27). The average grain size reported by the BM is 6μm (Fig. 2a) and the grains are observed to display mostly (78%) low angle grain boundaries (LAGBs) with misorientation less than 15° (refer Fig. 2c).

The specimen formed at 300 RPM (Ti-G2 300) shows slightly more refined grains (~10% of grains are $< 1\mu m$) than the BM (~5% of grains are $< 1\mu m$) (Fig. 2d). The average grain size is 5μm (Fig. 2e). The misorientation of grains in Ti-G2 300 is of 70% LAGBs and 30% high-angle grain boundaries (HAGBs).

The IPF map observed for the 450 RPM specimen (Fig. 2g) displays a considerably coarser grain structure when compared to the BM. A significantly higher average grain size of 10μm is demonstrated in Fig. 2(h). The Ti-G2 450 sample (Fig. 2i) displays 62 and 38% fractions of LABs and HAGBs respectively.

The IPF map 600 RPM (Ti-G2 600) specimen are presented in Fig. 2(j). The average grain size for Ti-G2 600 is 6μm with 5% of grains being $< 1\mu m$ (Fig. 2k). The grain misorientation is 70% of LAGBs (Fig. 2l).

None of the misorientation plots (Fig. 2c, f, i, and l) show traces of ~65 and 85° grains which are considered to be the preferential orientation of deformation twins in commercially pure Ti (Ref 28).

The EBSD analysis showed that the grains are oriented along the vertical step-down direction of the SPIF tool (indicated with arrow heads in Fig. 2d, g, j). In general, the SPIF processed Ti-G2 samples show limited change in average grain size when compared to the BM. However, there did occur a limited local refinement due to an increase in the fraction of grains that have grain sizes $\leq 1\mu m$. This is specifically apparent in the Ti-G2 300 sample when compared to the BM. The fraction of these smaller grains ($<1\mu m$) is similar for the BM and Ti-G2 600. The intermediate spindle speed 450 RPM sample did however display a coarser grain size than both the BM and the samples prepared at 300 and 600 RPM. A similar increase in average grain size for an intermediate set of process parameters was also reported by Shrivastava and Tandon (Ref 29) when conducting SPIF on commercially pure aluminum. They reported that during SPIF, the sheet metal blank undergoes stretching and strain hardening, which will result in a fine and stretched grain structure (increase in aspect ratio of grains), which is potentially a function of its process parameters.

3.2 X-ray Diffraction and Texture Analysis

X-ray diffractograms of the BM and the Ti-G2 processed samples are shown in Fig. 3(a-d). The peaks observed are of mostly α-Ti. Peak shift (toward the low angle side of 2θ) is significant (refer the peak intensity) while the broadening of peaks is marginal when comparing the SPIF samples with the BM (refer Fig. 3a-d). The peak shift is attributed to strain accumulation whereas the broadening of peak is due to grain refinement (Ref 30). Because the SPIF process involves stretching and strain hardening, an increase in dislocation density is potentially possible. To evaluate the dislocation density (area) for the SPIF samples an XRD peak broadening analysis (XRDPBA) was conducted utilizing the Williamson–Hall (W-H) method. Parameters including crystal size and lattice strain are obtained from the W-H method and is explained in the work of Zak et al. (Ref 31) and Krishna et al. (Ref 32). The parameters obtained from the XRDPBA are used to obtain the dislocation density by substituting into equation 1(Ref 33):

$$\rho = \sqrt{\rho_D \times \rho_S} \quad \text{(Eq 1)}$$

where ρ_D - dislocation density because of domain size, $\rho_D = \left(\frac{3}{D^2}\right)$ and ρ_S - dislocation density due of strain broadening,

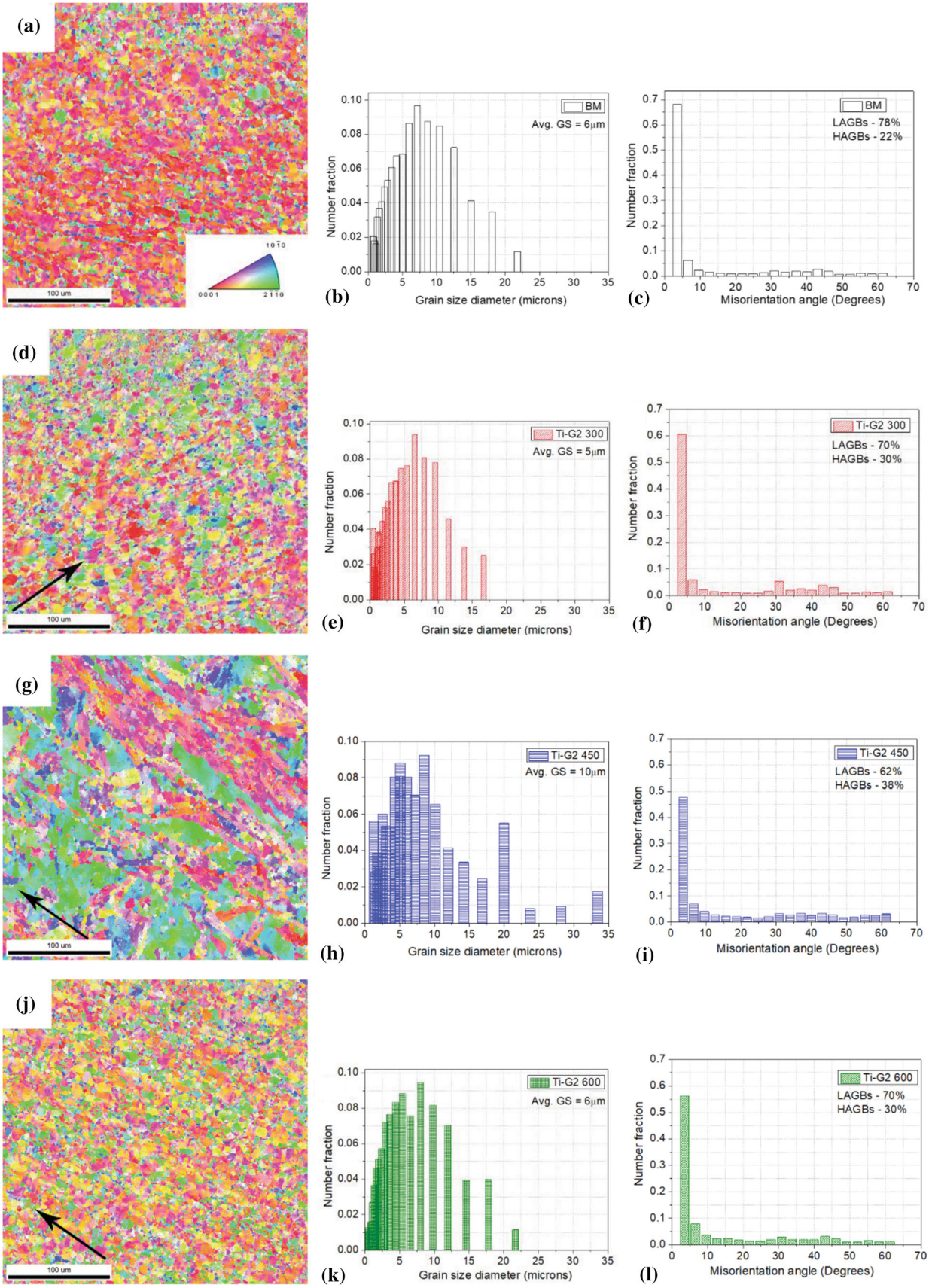

Fig. 2 IPF maps, grain size distribution and misorientation plot are given in order for: (a, b, c) BM, (d, e, f) Ti-G2 300, (g, h, i) Ti-G2 450, (j, k, l) Ti-G2 600. (inset in Fig. (a) represents the standard stereographic triangle)

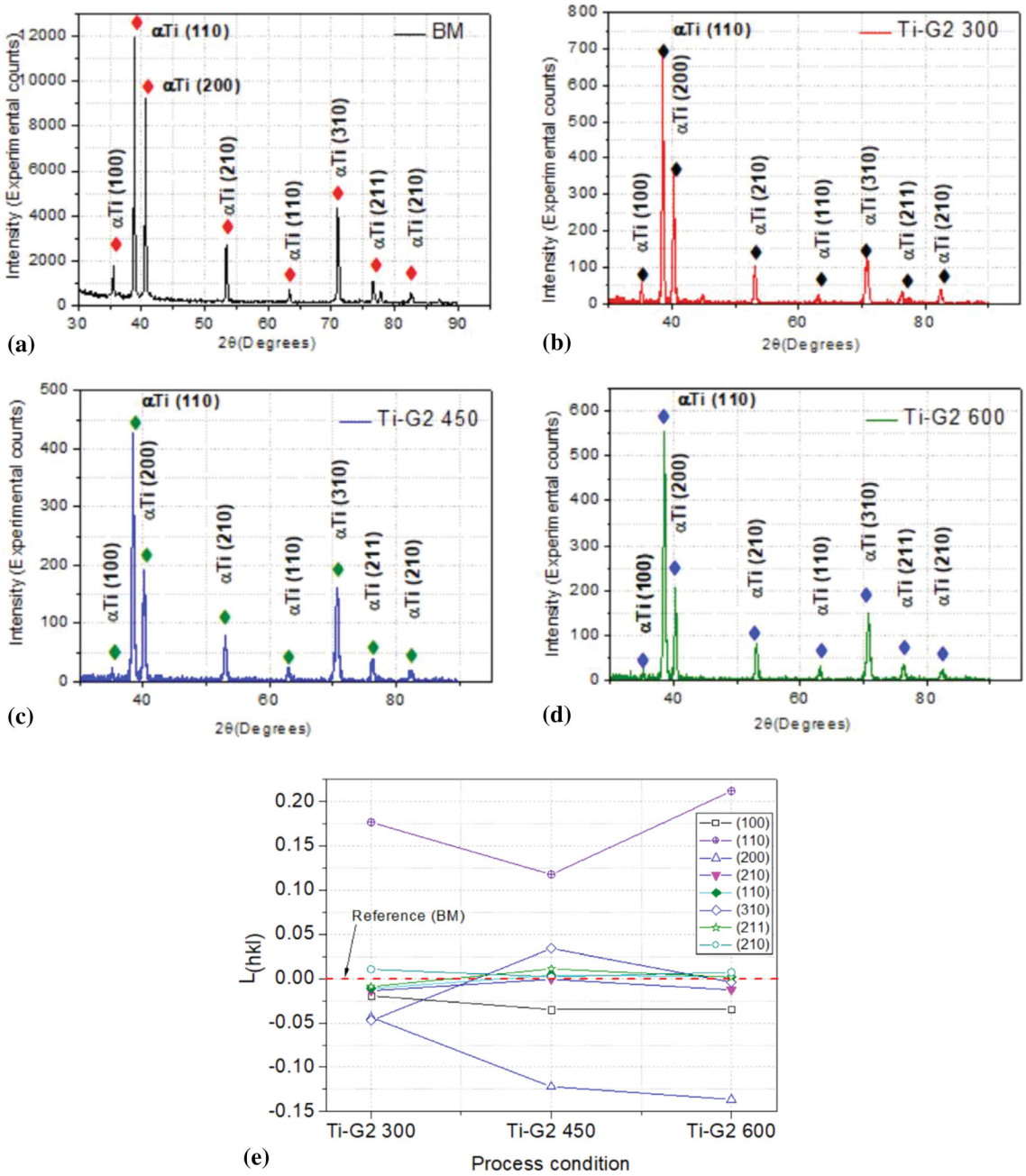

Fig. 3 X-ray diffraction patterns of: (a) BM, (b) Ti-G2 300, (c) Ti-G2 450, (d) Ti-G2 600, and (e) Lotgering factor (L_{hkl}) against process condition

$\rho_S = \left(\frac{K\varepsilon^2}{b^2}\right)$. Also $K = 6\pi$ and the Burgers vector is $b = 0.3249nm$ (Ref 34). D and ε denotes the crystallite size and lattice strain, which are also obtained from XRDPBA.

The dislocation densities for the BM material and the SPIF samples obtained from XRD are shown in Table 1. It clearly shows that compared to the BM the dislocation density increased significantly when subjected to the incremental forming process. The dislocation density also increased as a function of spindle speed with the highest and lowest densities being demonstrated for the commensurate highest and lowest spindle speeds.

IPF maps displaying grain orientation (texturing) are shown in Fig. 2(d), (g), and (j) for the SPIF processed samples at the different spindle speeds. To investigate the texturing, an attempted is made by utilizing the Lotgering factor (L_{hkl}). The Lotgering factor determines the preferred orientation of particular crystal planes, when compared with its coarse grain parent material. The L_{hkl} factor of various crystal planes for the

Table 1 Dislocation density values obtained through XRDPBA against various process conditions

Process condition	Dislocation density (10^{14},m^2)
BM material	0.63
Ti-G2 300	5.95
Ti-G2 450	9.22
Ti-G2 600	9.37

SPIF samples is presented in Fig. 3(e). The L_{hkl} factor is obtained from the work of Hajizadeh and Eghbali (Ref 35), which are as follows:

$$L_{(hkl)} = \frac{P_{(hkl)} - P^{R}_{(hkl)}}{1 - P^{R}_{(hkl)}} \quad \text{(Eq 2)}$$

$$P_{(hkl)} = \frac{I_{(hkl)}}{\Sigma I_j} \quad \text{(Eq 3)}$$

$$P^{R}_{(hkl)} = \frac{I^{R}_{(hkl)}}{\Sigma I^{R}_j} \quad \text{(Eq 4)}$$

where. $I_{(hkl)}$ denotes the intensity of the diffraction peak in the processed material, $I^{R}_{(hkl)}$ signifies the intensity of the diffraction peak of the reference material (mostly, annealed – coarse grained material). I_j and I^{R}_j are the intensities of any diffraction peak in the processed and reference material, respectively. $L_{(hkl)}$, the Lotgering factor, stipulates the difference in orientation of crystal planes among the processed material. An increase in $L_{(hkl)}$ implies a higher variation in crystal orientation. By implication if $L_{(hkl)} = 0$, then there exists no crystal orientation variation between the reference material and processed material. The dashed line in Fig. 3(e) represents the BM and acts as reference. Fig. 3(e) shows that planes (110) and (200) are significantly affected by the forming process and is furthermore also affected by spindle speed.

Figure 3(e) shows that preferred orientation has taken place in the Ti-G2 while varying the spindle speed. Through SEM-EBSD, the obtained pole figures of the BM, Ti-G2 300, Ti-G2 450 and Ti-G2 600 are shown in Fig. 4(a-d), respectively. The texture was recorded on the same location, which was used to record the IPF maps shown in Fig. 2. The pole figures (experimental) of (0 0 0 1) – basal plane, (1 0 $\bar{1}$ 1)–prismatic plane and (2 $\bar{1}$ $\bar{1}$ 0)–pyramidal plane is documented in this study. Figure 4(a) represents the initial texture of the BM and the (0 0 0 1) pole figure represents the c-axis of basal plane, in which the majority of grains are oriented at an angle of—30 to—60° along the transverse direction (TD–notated as A1 in pole figure) to field direction (FD–notated as A2 in pole figure). This preferred orientation of the basal plane is parallel to the initial rolling direction of Ti-G2 sheet metal, whereas the (1 0 $\bar{1}$ 1)and (2 $\bar{1}$ $\bar{1}$ 0) pole figures, representing the a–axis of material, display no preferred orientation (random texture). Similar rolling textures were observed in the BM of commercially pure Ti (Ref 36), in which the basal plane showed preferred orientation and the prismatic and pyramidal planes showed no preferred orientation. The texture intensities for different planes for the BM and the formed samples are reported as contour plots in Fig. 4. Ti-G2 300 (refer Fig. 4b) and Ti-G2 450 (refer Fig. 4c) display a significant weakening of texture along with a corresponding reduction in texture intensity compared to the BM. This is attributed to the induced shear deformation during SPIF, which resulted in a change in the microstructure. This texture intensity value however increases with increasing spindle speed. Ti-G2 600 displayed the maximum texture intensity amongst the different spindle speeds which is also higher than the texture intensity value of BM. This is because the texture in basal plane is dominant (refer to (0001) pole figures in Fig. 4) in the case of BM and Ti-G2 600. Parallelly, this can be visualized from the IPF maps of BM and Ti-G2 600 shown in Fig.2, which show predominantly (0001) oriented grains (large area of red coloured grains is evidenced). These grains are the indication for the evolution of stable orientation during plastic deformation towards the basal plane. However, this stable orientation is not observed in the case of Ti-G2 300 and Ti-G2 450. Among the three pole figures, the basal plane pole figure is dominant and exhibiting preferred orientation. The sample for Ti-G2 600 displays particularly a strong orientation of basal texture. Beausir et al. (Ref 37) identified five significant textural components including P, B, Y, C1 and C2 when deforming HCP metal plastically, When comparing the prismatic pole figure (refer Fig. 4) with its ideal pole figure (Ref 37), the increase in texture intensities near the ideal locations on the pole figure confirms the presence of P type texture and the formation near B type texture. The present results correlate closely with the report of Qarni et al. (Ref 36), where commercially pure Ti subjected to incremental equal channel angular pressing (i-ECAP) showed a strong P texture and B type texture.

3.3 Tensile Properties

Engineering stress–strain plot for the BM and the formed samples are shown in Fig. 5. The BM demonstrated a total elongation (TE) of 45% with an ultimate tensile strength (UTS) of 305 MPa. The Ti-G2 300 sample displayed a 26% higher UTS and a 59% reduction in TE when compared to the BM. The Ti-G2 450 sample displayed a 54% higher UTS and a 53% reduction in TE and the Ti-G2 600 sample a 79% higher UTS and a 73% reduction in TE. This clearly indicates that the forming process increases the UTS and reduces the elongation. This is typical for of most of the forming processes. The results do however also indicate that the UTS and the elongation are functions of spindle speed. An increase in spindle speed increases the UTS while it correspondingly reduces the total elongation. The increase in strength proportional to the spindle speed is attributed to the effect of dislocation accumulation due to the SPIF process. During plastic deformation, the density of obstacles to the dislocation movement increases. These include dislocations, grain refinement, twinning and mechanical fibering that all resists plastic deformation and enhances the strength of the material (Ref 38). The highest dislocation density was measured for the Ti-G2 600 sample which is commensurate with its highest tensile stress. As the reduction in grain size is not significantly affected spindle speed (see "Microstructural Characterization" Section), the predominant increase in strength must be due to the pile up of dislocations. The influence of the strong basal texture (Fig. 4(b-d) of (0001) pole figure) with predominantly P type orientation is also responsible for an enhancement in strength for the formed samples. Amongst the formed samples Ti-G2 600 displays a strong P type and B type texture with distinct texturing, which also displayed the highest dislocation density. Dislocation pile-up strengthening as well as the strong basal texture therefore has resulted in the highest tensile strength properties for Ti-G2 600. In line with the above various authors (Ref 38, 39) have reported enhanced mechanical properties for titanium due to the presence of a strong basal texture. An increase in spindle speed produces a significant change in grain orientation of basal planes, which supports an enhancement in strength. Although the BM holds high texture intensity than Ti-G2 300 and Ti-G2 450 it showed reduced tensile strength. This is because as the BM was subjected to tensile loading along its rolling direction

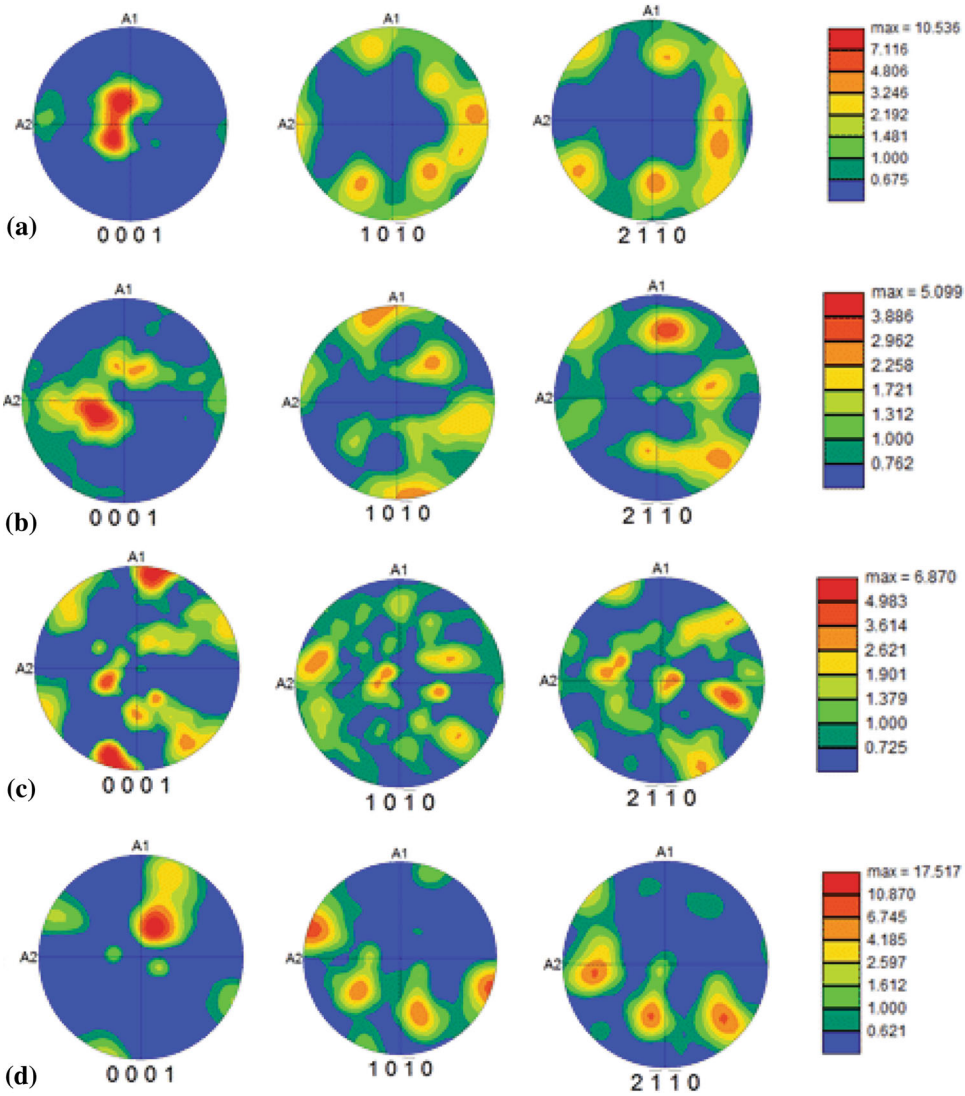

Fig. 4 Pole figures representing the formation of texture in the basal plane (0001), prismatic plane (1 0 $\bar{1}$ 1 1) and pyramidal plane (2 $\bar{1}$ $\bar{1}$ 0) for: (a) BM, (b) Ti-G2 300, (c) Ti-G2 450 and (d) Ti-G2 600. (The colour scale denotes the intensities of textures to the corresponding condition.)

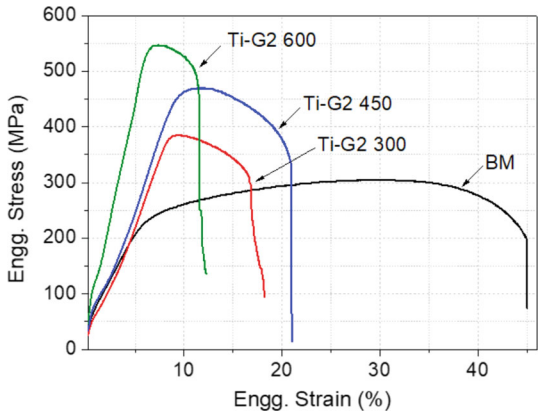

Fig. 5 Engineering stress–strain plot for the BM, Ti-G2 300, Ti-G2 450 and Ti-G2 600 (The tensile samples were obtained from the walls of frustum cups, which were processed with varied spindle speeds as 300, 450 and 600 RPM.)

(longitudinal direction), whereas the tensile samples obtained from the walls of the frustrum cups (refer to Fig. 1c) were transverse to the initial rolling direction. Hence, a monotonic increase in tensile strength is observed in the case of Ti-G2 300, Ti-G2 450 and Ti-G2 600 when compared to BM. In support to the present investigation, Bache and Evans (Ref 40) also reported superior tensile strength in the Ti alloy subjected to tensile loading along the transverse direction when compared to highly textured Ti alloy subjected to tensile loading along the longitudinal direction. Further, the aforementioned authors evidenced the variation in tensile strength irrespective of its texture intensity according to the direction of principal stress relative to the basal plane texture. The tensile loading in transverse direction acts perpendicular to basal plane texture lying conjunction with the longitudinal–short transverse plane promoted additional tensile strength in Ti alloys. Hence, the monotonic increase in the strength irrespective of texture intensity may be due to the influence of loading direction.

3.4 Limitations and Future Scope

The current investigation has shown that the number of HAGBs are increased with an increase in spindle speed (Fig. 2c, f, i and l). It may therefore be possible to further increase the HAGBs with a commensurate increase in spindle speeds. Similarly, an increase in the number of ECAP passes also resulted in more HAGBs. Furthermore, Ti-G2 exhibits dynamic recrystallization at elevated temperatures (Ref 36). If the spindle speed is increased further ($>$ 600 RPM), this may induce additional frictional heat to promote dynamic recrystallization. A suitable vertical step down can enhance deformation which may then lead to the fragmentation of the new grains as suggested by Mashinini et al. (Ref 41). The dynamic recrystallization is a recovery process due to deformation; the dislocations accumulate inside the grains and form sub-grains with LAGBs. On further straining, with high spindle speeds along with a suitable vertical step down, the probability for the rotation of sub grains and the misorientation increases ($>$ 15°) and creates new smaller grains around HAGBs (Ref 36, 42). As the already present HAGBs acts as nucleating sites for the sub grains, it is believed that grain refinement occurs at the outer edges of coarse grains and spreads towards inwards. It is therefore possible that a further increase in spindle speed along with a suitable vertical step down may promote further grain refinement in Ti-G2, which may enhance the mechanical properties further .

4. Conclusions

Single-point incremental forming (SPIF) was used to manufacture frustum cups from titanium grade 2 (Ti-G2) 1 mm sheet metal. A uniform wall angle of 55° was selected with forming continuing util fracture occurred at the edges. The spindle speed was varied between 300, 450 and 600 RPM. The vertical step down and feed rate were kept constant at 0.2 mm and 300 mm\min, respectively. Grease was used as lubricant.

The investigation has resulted in the following conclusions:

- The grains were oriented along the direction of vertical step down and were elongated along the same direction. An increase in spindle speed (tool rotational speed) has no significant effect on grain size.
- An increase in spindle speed resulted in a commensurate increase in strain hardening due to a proportional increase in dislocations density. The dislocation density at a spindle speed of 600 RPM displayed an increased from 0.63 $\times 10^{14}$\m^2 for the BM to 9.37$\times 10^{14}$\m^2.
- The preferred orientation of the crystal planes was identified by the Lotgering factor and further confirmed through texture studies based on electron-backscattered diffraction. An increase in spindle speed weakened the base metal texture initially; however, the basal plane texture was intensified. A further increase in spindle speed to its maximum level resulted in a strong basal texture and an enhanced texture intensity along with increased intensity of grains near P type and B type textures.
- Tensile testing indicates that the forming process increases the UTS and reduces the elongation. The results indicate that the UTS and the elongation are functions of spindle speed. An increase in spindle speed increases the UTS while it correspondingly reduces the total elongation. The accumulation of dislocations and formation of strong basal plane texture were identified as the potential reasons for the increment in strength.
- The results indicate that a significantly enhanced (compared to the BM) tensile strength of 550 MPa along with a 12% elongation is achievable by utilizing a spindle speed of 600 RPM during SPIF of Ti-G2 titanium sheet.

Acknowledgments

The authors would like to thank Professor Indradev Samajdar, Department of Metallurgical Engineering and Materials Science, National facility, OIM and Texture lab, A DST–IRPHA project, IIT-Bombay, India, for providing EBSD facility. Authors G.Y and S.V extend their gratitude to Dr. R. Narayanasamy, Professor–HAG (retired) and Dr. C. Sathiya Narayanan, Associate Professor, Department of Production Engineering, National Institute of Technology, Tiruchirappalli, Tamil Nadu, India for their technical inputs in the field of study.

Author Contributions

GY Concept, Experiment, Characterization. **SV** Analysis, Manuscript preparation–original draft. **RP** Validation. **MAR, AA** and **RFL** Review and editing of original draft.

Funding

No funds were received.

Data Availability

The experimental datasets obtained from this research work and then the analyzed results during the current study are available from the corresponding authors on reasonable request.

Declarations

Conflict of interest

The authors declare that they have no conflict of interest

Human and Animal Rights

The present work was not conducted on human or on any animals.

Consent for Publication

We confirm that the manuscript has been read and approved by all the authors and there are no other persons who satisfied the criteria for authorship but are not listed. We further confirm that all the authors listed in the manuscript has been approved by all of us.

References

1. D. Banerjee and J.C. Williams, Perspectives on Titanium Science and Technology, *Acta Mater*, 2013, **61**, p 844–879
2. J.L. Buckner, S.W. Stafford and D.M. Cone, Microstructural Characterization of Ti-6Al-4V X-Links from The Space Shuttle Columbia, *Mater Charct*, 2017, **131**, p 261–265
3. K. Mertová, P. Salvetr and M. Duchek, Comparison of Cryogenic and Cold Deformation of Commercially Pure Titanium, *Mater Today Proc*, 2020, **28**, p 916–919
4. Y.S. Kim, B.H. Lee and S.H. Yang, Prediction of Forming Limit Curve for Pure Titanium Sheet, *Trans Nonferrous Met Soc China*, 2018, **28**(2), p 319–327
5. F.K. Chen and K.H. Chiu, Stamping Formability of Pure Titanium Sheets, *J Mater Process Technol*, 2005, **170**(1–2), p 181–186
6. A.L. Port, F. Toussaint and R. Arrieux, Finite Element Study and Sensitive Analysis of the Deep-Drawing Formability of Commercially Pure Titanium, *Int J Mater Form*, 2009, **2**, p 121–129
7. P.A. Grün, E.H. Uheida, L. Lachmann, D. Dimitrov and G.A. Oosthuizen, Formability of Titanium Alloy Sheets by Friction Stir Incremental Forming, *Int J Adv Manuf Technol*, 2018, **99**, p 1993–2003
8. A. Daleffe, L. Schaeffer, D. Fritzen and J. Castelan, Analysis of the Incremental Forming of Titanium F67 Grade 2 Sheet, *Key Eng Mater*, 2013, **554–557**, p 195–203
9. G. Yoganjaneyulu, C. Sathiya Narayanan and R. Narayanasamy, Investigation on the Fracture Behavior of Titanium Grade 2 Sheets by using The Single Point Incremental Forming Process, *J Manuf Process*, 2018, **35**, p 197–204
10. G. Hussain, M. Ilyas, B.B.L. Isidore and W.A. Khan, Mechanical Properties and Microstructure Evolution in Incremental Forming of AA5754 and AA6061 Aluminum Alloys, *Trans. Nonferrous Met. Soc. China*, 2020, **30**, p 51–64
11. H. Wei, L. Zhou, B. Heidarshenas, I.K. Ashraf and C. Han, Investigation on the Influence of Springback on Precision of Symmetric-Cone-Like Parts in Sheet Metal Incremental Forming Process, *Int J Lightweight Materi Manuf*, 2019, **2**(2), p 140–145
12. T. McAnulty, J. Jeswiet and M. Doolan, Formability in Single Point Incremental Forming: A Comparative Analysis of the State of the Art, *CIRP J Manuf Sci Technol*, 2017, **16**, p 43–54
13. Ham M, Jeswiet J (2006) Single Point Incremental Forming and The Forming Criteria for AA3003. CIRP Annals – Manuf Technol 55: 241–244
14. T.A. Marques, M.B. Silva and P.A.F. Martins, On the Potential of Single Point Incremental Forming of Sheet Polymer Parts, *Int J Adv Manuf Technol*, 2012, **60**, p 75–86
15. G. Hussain, H.R. Khan, L. Gao and N. Hayat, Guidelines for Tool-size Selection for Single-point Incremental Forming of an Aerospace Alloy, *Mater Manuf Process*, 2013, **28**, p 324–329
16. G. Yoganjaneyulu and C. Sathiya Narayanan, A Comparison of Fracture Limit Analysis on Titanium Grade 2 and Titanium Grade 4 Sheets During Single Point Incremental Forming, *J Fail Anal Prev*, 2019, **19**, p 1286–1296
17. S. Golabi and H. Khazaali, Determining Frustum Depth of 304 Stainless Steel Plates With Various Diameters and Thicknesses by Incremental Forming, *J Mech Sci Technol*, 2014, **28**, p 3273–3278
18. G. Centeno, I. Bagudanch, A.J. Martnez-Donaire, M.L. Garca-Romeu and C. Vallellano, Critical Analysis of Necking and Fracture Limit Strains and Forming Forces in Single-point Incremental Forming, *Mater Des*, 2014, **63**, p 20–29
19. G. Ambrogio and F. Gagliardi, Temperature Variation During High Speed Incremental Forming on Different Lightweight Alloys, *Int J Adv Manuf Technol*, 2015, **76**, p 1819–1825
20. G. Vignesh, C. Sathiya Narayanan, C. Pandivelan, K. Shanmugapriya, B.N. Tejavath and L. Tirupathi, Forming, Fracture and Corrosion Behaviour of Stainless Steel 202 Sheet Formed By Single Point Incremental Forming Process, *Mater Res Express*, 2019, **6**(12), p 126540
21. D. Xu, W. Wu, R. Malhotra, J. Chen, B. Lu and J. Cao, Mechanism Investigation for the Influence of Tool Rotation and Laser Surface Texturing (LST) on Formability in Single Point Incremental Forming, *Int J Mach Tools Manuf*, 2013, **73**, p 37–46
22. G. Hussain, L. Gao and Z.Y. Zhang, Formability Evaluation of a Pure Titanium Sheet in the Cold Incremental Forming Process, *Int J Adv Manuf Technol*, 2008, **37**, p 920–926
23. J. Naranjo, V. Miguel, A. Martínez, J. Coello, M.C. Manjabacas and J. Valera, Influence of Temperature on Alloy Ti6Al4V Formability During the warm SPIF Process, *Proc Eng*, 2017, **207**, p 866–871
24. J. Adamus and P. Lacki, Possibility of the Increase in Titanium Sheets' Drawability, *Key Eng Mater*, 2013, **549**, p 31–38
25. V.C. Ajay, Parameter Optimization in Incremental Forming of Titanium Alloy Material, *Trans Indian Inst Met*, 2020, **73**(9), p 2403–2413
26. N. Nadammal, S.V. Kailas and S. Suwas, A Bottom-Up Approach for Optimization of Friction Stir Processing Parameters; A Study on Aluminium 2024–T3 Alloy, *Mater Des*, 2015, **65**, p 127–138
27. D. Shore, L.A.I. Kestens, J. Sidor, P. Van Houtte and A. Van Bael, Process Parameter Influence on Texture Heterogeneity in Asymmetric Rolling of Aluminium Sheet Alloys, *Int J Mater Form*, 2018, **11**, p 297–309
28. N. Stanford, U. Carlson and M.R. Barnett, Deformation Twinning and the Hall-Petch Relation in Commercial Purity Ti, *Metall Mater Trans A*, 2008, **39**(4), p 934–944
29. P. Shrivastava and P. Tandon, Microstructure and Texture Based Analysis of Forming Behavior and Deformation Mechanism of AA1050 Sheet During Single Point Incremental Forming, *J Mater Process Technol*, 2019, **266**, p 292–310
30. T. and Unga´r, Microstructural Parameters from X-ray Diffraction Peak Broadening, *Scripta Mater*, 2004, **51**, p 777–781
31. A.K. Zak, W.H.A. Majid, M.E. Abrishami and R. Youse, X-ray Analysis of ZnO Nanoparticles by Williamson-Hall and Size-Strain Plot Methods, *Solid State Sci*, 2011, **13**, p 251–256
32. K.S.V.B.R. Krishna, S. Vigneshwaran, K. Chandra Sekhar, S.S.R. Akella, K. Sivaprasad, R. Narayanasamy and K. Venkateswarlu, Mechanical behavior and Void Coalescence Analysis of Cryorolled AA8090 Alloy, *Int J Adv Manuf Technol*, 2017, **93**, p 253–259
33. R.R. Smallman and C.H. Westmacott, Stacking Faults In Face-Centred Cubic Metals and Alloys, *Philos Mag*, 1957, **2**, p 669–683
34. Y.T. Prabhu, K.V. Rao, V.S. Sai Kumar and B. Siva Kumari, X-Ray Analysis by Williamson-Hall and Size-Strain Plot Methods of ZnO Nanoparticles with Fuel Variation, *World J Nano Sci Eng*, 2014, **4**, p 21–28
35. K. Hajizadeh and B. Eghbali, Effect of Two-Step Severe Plastic Deformation on the Microstructure and Mechanical Properties of Commercial Purity Titanium, *Metal Mater Int*, 2014, **20**(2), p 343–350
36. M.J. Qarni, G. Sivaswamy, A. Rosochowski and S. Boczkal, On The Evolution of Microstructure and Texture in Commercial Purity Titanium During Multiple Passes of Incremental Equal Channel Angular Pressing (I-ECAP), *Mater Sci Eng A*, 2017, **699**, p 31–47
37. Beausir B, Suwas S, To´th LS, Neale KW, Fundenberger JJ (2008) Analysis of Texture Evolution in Magnesium During Equal Channel Angular Extrusion. Acta Mater 56: 200–214
38. H.N. Abarbekoh, R. Abbasi, A. Ekrami and A.A.Z. Moayyed, Notch-Texture Strengthening Mechanism in Commercially Pure Titanium Thin Sheets, *Mater Des*, 2014, **55**, p 683–689
39. Z.S. Zhu, R.Y. Liu, M.G. Yan, C.X. Cao, J.L. Gu and N.P. Chen, Texture Control and The Anisotropy of Mechanical Properties in Titanium Sheet, *J Mater Sci*, 1997, **32**, p 5163–5167
40. M.R. Bache and W.J. Evans, Impact of Texture on Mechanical Properties in an Advanced Titanium Alloy, *Mater Sci Eng A*, 2001, **319–321**, p 409–414
41. P.M. Mashinini, I. Dinaharan, J.D.R. Selvam and D.G. Hattingh, Microstructure Evolution and Mechanical Characterization of Friction Stir Welded Titanium Alloy Ti–6Al–4V Using Lanthanated Tungsten Tool, *Mater Charact*, 2018, **139**, p 328–336
42. R.D. Doherty, D.A. Hughes, F.J. Humphreys, J.J. Jonas, D.J. Jensen, M.E. Kassner, W.E. King, T.R. McNelley, H.J. McQueen and A.D. Rollett, Current Issues In Recrystallization: A Review, *Mater Sci Eng A*, 1997, **238**(2), p 219–274